





Cite this: *Phys. Chem. Chem. Phys.*,
2017, **19**, 11869

Unexpected proton mobility in the bulk phase of cholinium-based ionic liquids: new insights from theoretical calculations

Marco Campetella,[†] Maria Montagna,[‡] Lorenzo Gontrani,[‡]  Eleonora Scarpellini and Enrico Bodo *

We have explored by means of *ab initio* molecular dynamics two ionic liquids based on the combination of a choline cation with deprotonated cysteine and aspartic acid anions. While the combination of the strong base choline with various other amino-acids leads to the formation of a highly ionized medium where proton transfer is negligible, the presence of additional protic functions on the SH and COOH groups leads to an unexpected and interesting behavior and to a sizable migration of their acidic protons onto the NH₂ basic terminals. As far as we know this is the first time that such proton migration, which in water leads to the well-known zwitterionic form of aminoacids, is observed to take place in their ionized, anionic form. We analyze in detail such dynamical effects using accurate *ab initio* molecular dynamics computations validated through comparison with X-ray scattering data.

Received 16th February 2017,
Accepted 7th April 2017

DOI: 10.1039/c7cp01050h

rsc.li/pccp

1. Introduction

From a general point of view an ionic liquid (IL) is a substance made entirely by ionic couples that, due to it being liquid at room temperature, presents several specific properties¹ which make it an interesting subject of research due to its increasing number of possible technological and industrial applications.^{2–5} In addition, the low environmental impact of ILs (due to their negligible vapor pressure) makes them an optimal candidate to be used as benign and less harmful solvents in industrial processes. Given the huge number of anion–cation combinations, the possibility of providing ILs with special features has given them the reputation of “designer materials” whose properties can be tailored for specific applications. Of particular interest is the possibility of creating special ILs that are fully biocompatible. The implementation of these materials has opened new routes for their application in the pharmacological and biomedical fields and, in general, in green-chemistry processes.^{6–9} In this respect a new generation of ILs has been synthesized in which the typical inorganic anions such as [PF₆][−], [BF₄][−], Br[−], and Cl[−], have been substituted by organic amino acid anions.¹⁰

In this work we focus on two ILs consisting of a choline cation [Ch]⁺, mixed with two amino-acid anions:¹¹ cysteine

[Cys][−], and aspartic acid [Asp][−]. This class of ILs, given that both constituents play a role in metabolic processes, was proven to be nontoxic for humans and for the environment,^{12–14} and can be considered a promising class of materials for a wide range of bio-related applications.^{15–17}

Given that, formally, these liquids result from acid base reactions, they fall into a broad class of ILs called protic ILs (PILs).^{18–21} Despite the simplicity of the composing molecular ions, this class of ILs can show a very complex structural and dynamical behavior due to the occurrence of nano-segregation phenomena.^{22,23} In this particular set of ILs there is a noticeable and peculiar network of hydrogen bonds,²⁴ whose strength obviously depends on the ionic partners and their relative acidity.

In general, the degree of ionization in a PIL depends upon the ΔpK_a between the acid and the conjugate acid of the base.²⁵ The larger the ΔpK_a , the more ionized the final material. For very low ΔpK_a no proton transfer occurs and the system remains composed of neutral species. At higher values of ΔpK_a we have an intermediate situation where the proton is only partially transferred to the base.²⁶ Finally, when the ΔpK_a is sufficiently large the ensuing liquid is completely ionized. A system made by a choline cation ($pK_a \sim 13.9$) and an amino-acid ($pK_a \sim 2–2.4$) represents a typical situation falling in the third case (large ΔpK_a) where the final liquid medium is completely made by ionic partners. Such an ideal case can be easily treated and modeled *via* classical (topologically fixed) MD simulations.

In a completely ionized liquid (namely an IL) the charge transport is due to the ionic motion and its conductivity is

Chemistry Department, University of Rome “La Sapienza”, Piazzale A. Moro 5,
00185, Rome, Italy. E-mail: enrico.bodo@uniroma1.it

[†] Present address: Laboratoire LECIME, CNRS UMR-7575, Chimie-ParisTech,
11 rue P. et M. Curie, F-75231 Paris, France.

[‡] Present address: The Leibniz Institute of Polymer Research Dresden (IPF),
Hohe Str. 6, D-01069 Dresden, Germany.

inversely proportional to the viscosity of the fluid that is generally high leading to the well known, poor conducting behavior of many ionic liquids. Unfortunately, allowing proton diffusion by using an acid–base pair with smaller ΔpK_a usually further reduces the conductivity because the concentration of charge carriers (the ions) decreases. In addition a non-completed ionization reaction often leads to other problems such as phase separation and to a high volatility of the polar, non ionic phase. It is therefore of great relevance for electrochemistry the discovery of fluids where the degree of ionization is still complete (so that they maintain the useful properties ascribed to ILs) but proton diffusion could occur^{27,28} *via* other mechanisms.

The two PILs that are the subject of this study have an amino-acid anion that presents an additional protic function and proton transfer from these groups (–SH or –COOH terminals) to the –NH₂ terminal is possible. With this prescription the choline cations would remain simple spectators and therefore the cation choice may represent an additional, useful degree of freedom to further enhance or tailor specific properties. In order to allow the proton transfer we have to however face another additional problem: in ionic liquids the local, short-range geometry of the fluid is characterized by an alternating pattern of ions and counterions. Since both the acidic functions and the basic ones are located on the anion, for proton transfer to occur, two anions must be close enough in the fluid. This means that the molecular anions should present some sort of attractive interaction between each other. As we shall see, these interactions can be mediated by H-bonds.

Given the rather complex chemical morphology of the compounds we are dealing with, these systems have to be treated realistically only *via ab initio* molecular dynamics (AIMD) where the topology of the chemical bonds is not held fixed.

2. Methods

2.1 Computational methods

We have performed different AIMD simulations of the bulk system composed by an equal number of amino acid anions and [Ch]⁺ cations. Pre-equilibration was performed employing classical molecular dynamics within periodic boundary conditions, using the AMBER program package²⁹ and the Gaff force field.^{30,31} A 2 ns-long equilibration trajectory was produced for the two systems in the *NPT* ensemble; the simulation temperature was set at 350 K. The difference between MD and experimental density was less than 5%. The starting configurations obtained by this procedure were used to set up *ab initio* molecular dynamics simulations.

The [Ch][Cys] system has been modeled as described in ref. 32 using the program CP2K,³³ the Quickstep module³⁴ and the orbital transformation³⁵ for faster convergence. The electronic structure was calculated by means of the PBE³⁶ functional, with an explicit van der Waals correction that includes the empirical dispersion correction (D3) by Grimme.³⁷ Basis sets of the kind MOLOPT-DZVP-SR-GTH and GTH pseudopotentials^{38,39}

were used. The timestep was chosen to be 0.5 fs and the simulation temperature was set at 350 K using the Nose–Hoover thermostat⁴⁰ in order to slightly accelerate the dynamics which is very slow under ambient conditions due to the high viscosity of these systems.¹¹ The cell has a side-length of 25.6 Å and contains 56 ionic pairs; the production time was 24 ps with a constant density of 1.24 g cm^{−3} (the experimental value is 1.18 g cm^{−3}).

The [Ch][Asp] simulation has been instead performed using the CPMD⁴¹ code. The reason for the choice of the different MD paradigms was dictated by the different computational architectures that were employed for the computation and by the better scaling of the CPMD software on that architecture. In any case, we had shown that, in these kinds of systems, CP dynamics and BO dynamics provide essentially the same results.⁴² The cell of the [Ch][Asp] system has a side length of 18.0 Å and contains 16 ionic pairs. Car–Parrinello molecular dynamics has been performed employing the PBE functional and Troullier–Martin⁴³ pseudopotentials (PP) for first row elements. Production time was 56 ps at 300 K with a constant density of 1.07 g cm^{−3} (the experimental value is approximately 1.1 g cm^{−3} (ref. 44)). The trajectory post-processing and the investigation of structural properties have been carried out using the TRAVIS package⁴⁵ and “in house” software codes.

Ab initio calculations for the isolated molecules have been performed using Gaussian09.⁴⁶ Optimization has been performed at the PBE/6-311+G** and MP2/6-31+G** levels and harmonic frequencies have been computed in order to ensure the correct characterization of the critical points. ESP charges have been determined using the MP2/6-311++G(2d,2p) electronic density at the MP2/6-31G* geometry. The cluster calculations of the [Cys][Cho] system have been carried out using a two layer ONIOM scheme where the model system (a single [Cys] anion) has been treated as above using PBE and MP2 and the medium layer (the surrounding 4 [Cys] anions and 4 [Ch] cations) at the PBE/midi! level. The medium layer is identical for both isomers and has been held fixed during the geometry search to avoid spurious energy artifacts coming from conformational mobility. The cluster has been created by taking a snapshot of the MD trajectory and extracting the first 4 neighbor cations and anions along with the reference anion.

2.2 Experimental X-ray structural factors and their computation

For the synthesis of the [Ch][AA] ILs, we used, with slight variations, the method recently reported in the literature by our group¹¹ and we shall not report here the details.

The large angle X-ray scattering experiments were performed at room temperature using the non-commercial energy-scanning diffractometer built in the Department of Chemistry at the University ‘La Sapienza’ of Rome (Italian Patent No. 01126484-23 June, 1993). For a detailed description of the instrument, technique, and the experimental protocol of the data acquisition phase, the reader is referred to ref. 47–50 and specifically to these systems to ref. 32. The total intensity of the radiation scattered by the sample, after the correction for systematic effects and rescaled to absolute units (electron units per stoichiometric unit), can be expressed as the

sum of independent atomic scattering and of $I(Q)$, the 'static structure factor' that constitutes the structurally sensitive part of the scattered intensity due to the interference contributions. Q is the magnitude of the transferred momentum. The function $I(Q)$ is related to the atom-atom pair correlation functions, according to the formula:

$$I(Q) = \sum_{i=1}^N \sum_{j=1}^N x_i x_j f_i f_j \times \left[4\pi\rho_0 \int_0^\infty r^2 (g_{ij}(r) - 1) \frac{\sin Qr}{Qr} dr \right]$$

where ρ_0 is the bulk number density of the system, x_i are the numerical concentrations of the species and f_i the Q -dependent X-ray scattering factors. Both the experimental and theoretical structure functions have been multiplied by a modification function

$$M(Q) = \frac{f_N^2(0)}{f_N^2(Q)} \exp^{-0.01Q^2}$$

that is useful to improve the curve resolution at high Q . In the plots we shall always report the product $I(Q)M(Q)Q$.

3. Discussion and results

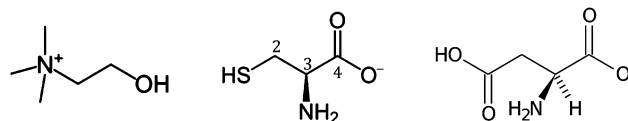
We had already provided in ref. 51 a preliminary study of choline-based ILs by focusing on their docking morphology for the isolated ionic couples in the gas phase. The results from a series of high quality *ab initio* simulations have clearly shown that the docking geometry of the compounds behaves in a very similar manner along the entire series. The main intermolecular bonding feature is a strong hydrogen bond between the OH group on $[\text{Ch}]^+$ and the carboxylate of the aminoacid. This bonding feature represents substantially the driving force of aggregation beyond the obvious electrostatic cohesive force. We have further confirmed these important results in a second and third study^{32,32} that focused on the behavior of the liquids obtained by a homologous series of molecular anions made by 11 different amino-acids. As we previously noticed in ref. 32, a peculiar case among those studied, is represented by the $[\text{Ch}][\text{Cys}]$ material where intra- and inter-molecular proton transfer occurs from the $-\text{SH}$ to the $-\text{NH}_2$ terminal.

An even more complicated liquid arises when mixing the $[\text{Ch}]^+$ cation with the $[\text{Asp}]^-$ amino-acid anion where we have a second carboxylic acid function. The systems under study and their chemical structures are shown in Scheme 1.

3.1 The simulation of the $[\text{Ch}][\text{Cys}]$ ionic liquid

$[\text{Ch}][\text{Cys}]$ is an IL that comes from the deprotonation reaction of an amino-acid with two acidic hydrogen atoms. As shown in ref. 11, the IL formation reaction can proceed with the abstraction of one proton (the one on the carboxylic acid) and form a completely ionized IL. The reaction can then be further continued removing also the second proton (the one on the $-\text{SH}$ terminal) and in this case a solid is obtained that has a melting point above 90° .

The liquid conductivity of $[\text{Ch}][\text{Cys}]$ is very likely due to a poor "Walden" mechanism since it linearly correlates with the



Scheme 1 Molecular components of the liquids under study: the choline cation on the left and the amino-acid anions on the right (deprotonated cysteine and aspartic acid respectively).

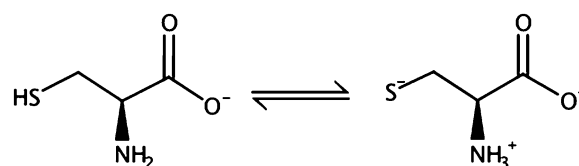
inverse of the viscosity, which is high.¹¹ It therefore follows that this liquid is not a candidate for fast proton transfer, nevertheless its microscopic structure turns out to be quite peculiar and points to a possible mechanism with which one could, in principle, obtain a neat, dry IL with conductivity mediated by proton transfer.

The existence of a relatively mobile proton on the $-\text{SH}$ moiety makes this system extremely complicated from the nanoscopic point of view. As we have already pointed out in ref. 42, during our simulations few $[\text{Cys}]$ anions underwent an intramolecular proton transfer from the $-\text{SH}$ terminal to the $-\text{NH}_2$ group (see Scheme 2). As we have already discussed in the aforementioned paper, the intramolecular proton transfer leads to the formation of a molecular ion with triple charge separation. We had found by simple gas phase computations that this zwitterionic anion (**Cys-Z**) turns out to be 2–4 kcal higher in energy than its ionic counterpart⁴² (**Cys-N**).

To further investigate this behavior, here we have repeated the computation of the relative energy of two isomers (**Cys-N** and **Cys-Z**) in the gas phase and in a solvent whose dielectric constant matches that of a typical protic ionic liquid ($\epsilon = 35.7$) using both the MP2/6-31+G** and the PBE/6-311+G** methods. In addition, and to simulate a more realistic environment with respect to a continuum model, we have also calculated the energy difference between the two isomers in a cluster of ionic couples made by a $[\text{Cys}]$ anion in both isomeric forms surrounded by 4 $[\text{Ch}][\text{Cys}]$ ionic couples.

The resulting MP2 optimized gas-phase structures of the two anionic isomers **Cys-N** and **Cys-Z** are reported in Fig. 1 along with the charge density colored with its electrostatic potential. The atomic charges obtained through an ESP (electrostatic potential fitting) procedure with the MP2/6-311++G(2d,2p) density are reported in Table 1 where we clearly see the change in the polarity of the functional group (compare with Fig. 1) upon isomerization.

The relative energy of the isomers and of the transition state between them is reported in Table 2 where we can see that in a solvent with a medium dielectric constant ($\epsilon = 35.7$, similar to typical protic ionic liquids⁵²) the relative stability of the



Scheme 2 Intramolecular proton transfer in the $[\text{Cys}]$ anion.

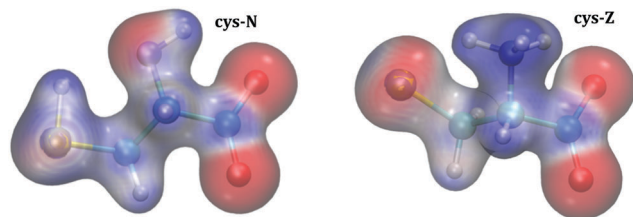


Fig. 1 [Ch][Cys]: optimized structures of the two isomers of the [Cys] anion with their charge density colored with the resulting electrostatic potential. Left: **Cys-N** (anionic form), right: **Cys-Z** (anionic-zwitterionic).

Table 1 Atomic charges of the two [Cys] isomers computed through the ESP procedure using the MP2 electronic density. For equivalent atoms, we have taken the average charge. The hydrogen atoms attached to carbon are not reported. For numbering see Scheme 1

Atom	MP2 atomic charges	Atom	MP2 atomic charges
Cys-N		Cys-Z	
S	-0.21	S	-0.77
C2	-0.09	C2	-0.22
C3	-0.26	C3	-0.26
C4	1.07	C4	1.00
O	-0.89	O	-0.83
H(S)	0.17		
N	-0.30	N	0.11
H(N)	0.09	H(N)	0.23

structures is reversed or at least attenuated with respect to the gas phase. Even without inversion of the relative stability, the MP2 energies (as computed in an average dielectric medium) predict that, at equilibrium, about 15% of the [Cys] anions would be in the **cys-Z** form. Thermodynamically both MP2 and DFT, although to a different extent, seem to point to the formation of the **cys-Z** forms. If we look at the kinetics of the isomerization process, we see that the calculated barrier to proton transfer is much higher for MP2 than for the pure PBE functional. This is a well-known deficiency of pure functionals such as PBE which typically underestimates activation barriers. On the other hand, MP2 methods are known to overestimate systematically barrier heights in H atom transfer reactions.⁵³ Anyway, even if the real barriers were more like MP2, they would still be low enough that we would expect to see a consistent transformation of the [Cys] anion from the **cys-N** to the **cys-Z** form. In other words, we believe that the PBE-based

MD trajectories described below should provide a perfectly valid qualitative description of the real system, the main difference being the timescale of the isomerization process that might turn out, owing to higher kinetic barriers, to be slower than the one described by our dynamics. The energetic preference for the **cys-Z** isomer is confirmed by the computations in the cluster environment. At the PBE level the **cys-N** directly converts to **cys-Z** during the optimization process. At the MP2 level the stability of the **cys-Z** form in the cluster environment is enhanced to more than 10 kcal mol⁻¹.

We now move to the description of the results that we can obtain from the AIMD simulations. We report in Fig. 2 the development of the S-H and N-H distances (within the same ion) in 6 selected molecules along the AIMD trajectory. As we can see, during the (limited) time span of our simulation we can easily identify at least four complete intramolecular proton transfers from the -SH to the -NH₂ group (panels 3, 4, 5 and 6 in reading order). In panel 1 we have reported an example where the proton is moving between the two basic groups *via* a strong H-bond between the resulting -NH₃⁺ and the -S⁻ terminals while in panel 2 we see instead a situation where the proton, initially on the -SH group, “jumps” back and forth on the amino group atom several times, giving rise to a complicated dynamics.

A typical ionic liquid generally exists in a mobile, but structured array of ions in which every cation is surrounded by anions and *vice versa*. The fact that the anions are generally separated by a cation limits the possibility of direct contacts between them. This is the reason why we see mostly intramolecular proton transfers. For the same reason, it is much more difficult to see an inter-anionic one. Despite the electrostatic repulsion, two anions may come in close contact if they have the possibility of forming a strong H-bond between the -SH and -NH₂ terminals.

To investigate this intriguing possibility, we report in Fig. 3 three radial distribution functions (RDFs) within the same anions and between different anions. In the left panel we report the RDFs for the N-H (black line) and S-H (red line) distances where we see the dominant S-H motifs (structure **cys-N**) with a typical S-H distance of 1.38 Å (see also Fig. 2) and the less occurring -NH₃⁺ motif (structure **cys-Z**) with an N-H distance of 1.06 Å. The **cys-Z** motif can also be identified by the second broader, weaker peak in the S-H RDF (red line) with a

Table 2 Relative energy between the optimized structures of the two isomers of [Cys] along with the energy of the inter-conversion barrier

Structure	ΔE gas-phase (kcal mol ⁻¹)		ΔE (solvent $\epsilon = 35.7$) (kcal mol ⁻¹)	
	MP2/6-31+G**	PBE/6-311+G**	MP2/6-31+G**	PBE/6-311+G**
Cys-N	0.0	0.0	0.0	0.0
Cys-Z	7.1	3.1	1.1	-1.7
TS	8.5	3.6	7.3	2.2
ΔE (cluster) (kcal mol ⁻¹)				
	MP2/6-31+G**	PBE/6-311+G**		
Cys-N	0.0	Conversion to Cys-Z		
Cys-Z	-12.0	—		

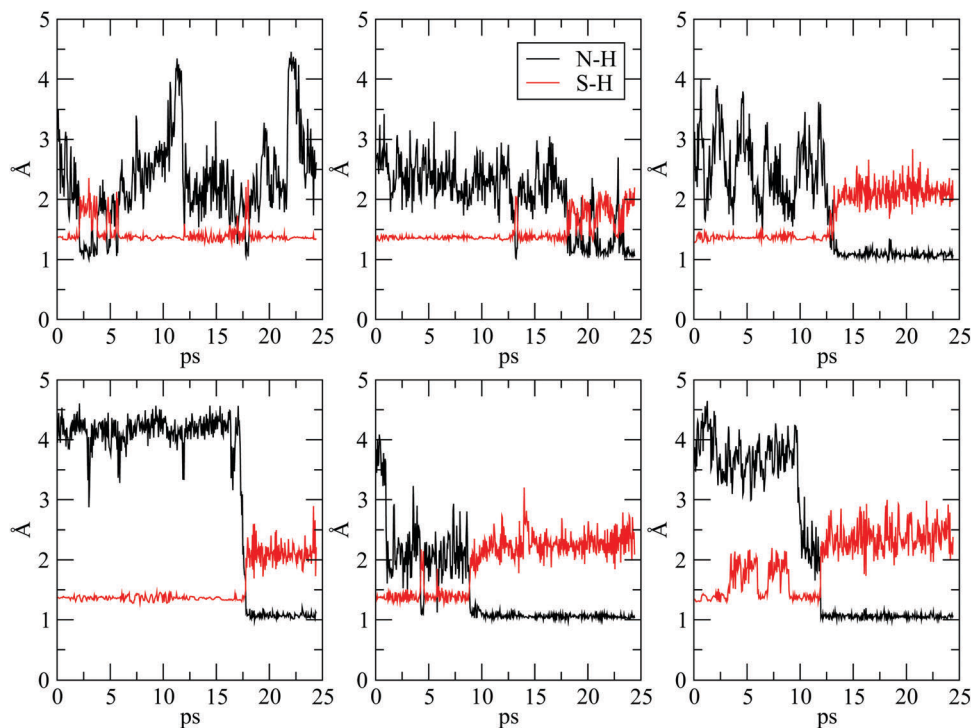


Fig. 2 [Ch][Cys]: N–H (black) and S–H (red) distances as a function of simulation time.

maximum slight above 2.0 Å which correspond to the distance of the S···H–N hydrogen bond occurrence seen in Fig. 2. On the right panel, instead, we report the inter-molecular (anion–anion) N–HS distance. The H-bond pattern already seen within the same anion is repeated here with a first peak at 1.11 Å pertaining to a **cys-Z** motif (with a S···H–N pattern) and a broader one at 1.8–1.9 Å due to the **cys-N** state (with an S–H···N pattern). This last example tells us clearly that several anions establish strong H-bonds between them.

Although we have found several occurrences of strong H-bonds between different anions, we show here a peculiar case where a complex proton transfer dynamics takes place between 3 different anions bound together by S–H–N H-bonds. The situation is graphically depicted in Fig. 4 where we report several snapshots of the simulations, but we draw only the three anions involved in the proton exchange. At the beginning of the simulations both active protons (colored in magenta in Fig. 4) are bound to the sulfur atom (panel 1) and the chemical environment is a (**cys-N**)₃ cluster. After 2 ps (panel 2) we see a first proton transfer from the anion on the left to the central one. After 3 ps (panel 3) the first proton has gone back to the sulfur atom while the one from the anion on the right has been transferred to the central one. Between 10 and 12 ps both protons are again on the two sulfur atoms (panel 4). At 12.5 ps the anion on the right undergoes an intramolecular proton transfer (panel 5) while the anion on the left transfers its proton to the central one (panel 6). After 24 ps, the system becomes a (**cys-N**)(**cys-Z**)₂ cluster.‡

‡ The additional proton that is transferred to the central molecule cannot be shown for graphical reason.

3.2 [Ch][Cys]: final remarks and experimental validation

Since [Ch][Cys] does not seem to be a particularly good current conductor,¹¹ it is very likely that the isomerization reaction from **cys-N** to **cys-Z** reaches a dynamic equilibrium and that the proton does not move through the ionic medium. It is possible that the event of interanionic proton transfer noticed above is only a sporadic event in the fluid not sufficient to sustain proton “jump” mechanisms apt to carry charge. The isomerization reaction is however an interesting and unexpected feature of this IL and strongly influences the local microscopic structure and properties of the liquid. As shown in ref. 11, the fact that some of the PILs based on choline and amino-acids (specifically [Cys], [Ser] and [Lys]) have much higher viscosities with respect to other members of the series has been attributed to their capacity of forming additional hydrogen bonds thanks to the heteroatom on the side chain. We believe that in these amino-acids the above isomerization reaction can take place (to various extents) and that this might play also a role in determining their dynamical behavior. In particular, the additional charge separation of the anionic–zwitterionic form might slow down ion diffusion and dynamics.

To support our theoretical results, we report in Fig. 5a a comparison between the calculated and measured $I(Q)M(Q)Q$ for the [Ch][Cys] system. As we can see the agreement between the theoretical and experimental patterns is excellent apart from the intermediate range region (medium values of Q in the graph). This discrepancy can be easily explained by assuming that the proton migration reaction and therefore the isomerization from the **cys-N** to the **cys-Z** form takes place in a time which can be substantially longer than our simulation time.

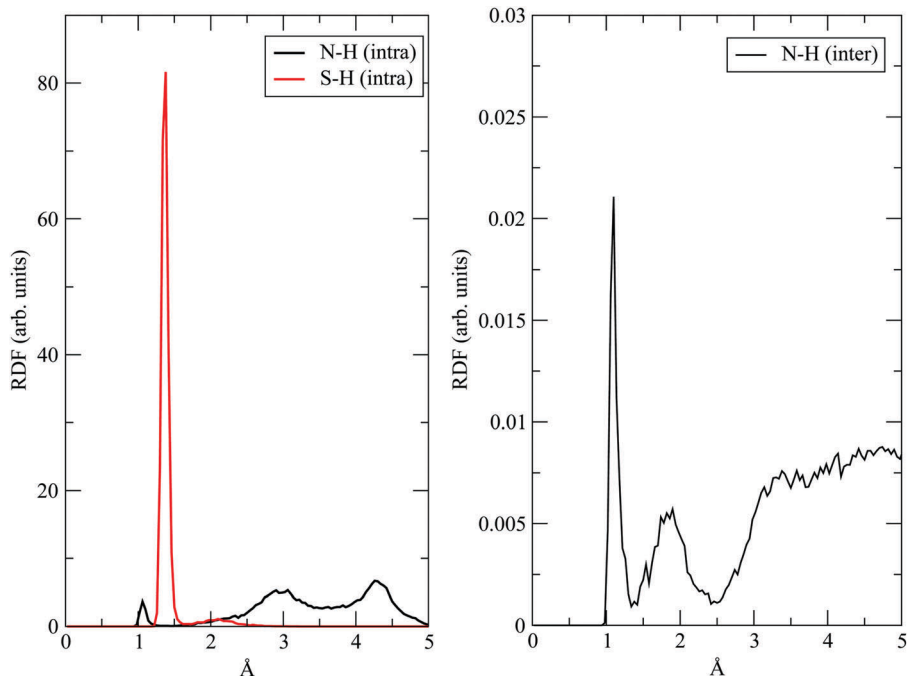


Fig. 3 [Ch][Cys]: left: radial distribution functions for intramolecular S–H and N–H contacts within the anion. Right: Intermolecular (anion–anion) N–H radial distribution functions.

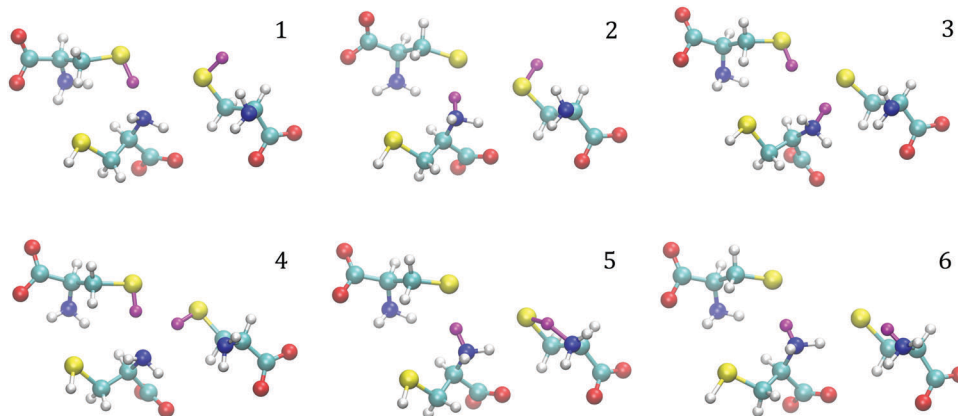


Fig. 4 [Ch][Cys]: sequential snapshots of the molecules taking part in the proton exchange.

What we are really sampling here with the simulation is a state of the fluid that has not yet reached the chemical equilibrium completely. The agreement with the experimental data in the short-range region (high Q values) however tells us clearly that the computations are able to grasp with great accuracy the positions of the electron-rich atoms, which, in turn, depend on the isomerization state of the single molecules.

3.3 The [Ch][Asp] system

As in the previous case of [Ch][Cys], here we have two different de-protonation sites at the two carboxylic acid terminals. The complete deprotonation (as for the [Cys] IL) gives rise to a solid even above 90° . Partial deprotonation instead leads to a compound that has been shown to be a glassy solid slightly above RT,¹¹ which turns into a viscous liquid at 90° . The first acid

group deprotonated is the most acidic one ($pK_a = 2.1$) in the α position; the second acid has a $pK_a = 3.9$. While in the previous case of [Ch][Cys] the additional protic function was a base, in this case we have an acid that has a much greater chance of donating protons. It must be kept in mind however that the basicity and acidity scales in ILs differ significantly from those in water owing to the radically different microscopic structure of the medium and its lower polarizability (hence the lower dielectric constant with respect to water). We have computed as we did for the [Cys] anion the relative energy and the barrier for the intramolecular proton transfer in an [Asp] anion. The energy differences are presented in Table 3 and the isomerization reaction in Scheme 3. Unlike the [Cys] case, here the proton transfer barrier is very low and the **asp-N** and **asp-Z** isomers are almost isoenergetic. From this data, one would

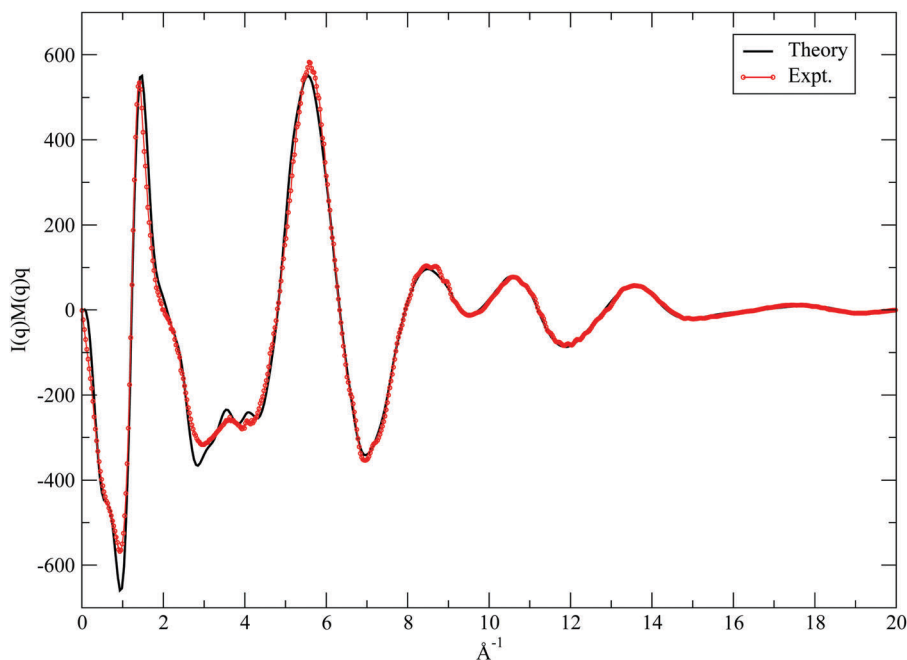


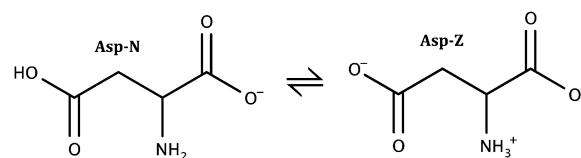
Fig. 5 Structural factors for the [Ch][Cys] system. Red: experimental data; black, computed results from AIMD simulation.

Table 3 Relative energy between the optimized structures of the two isomers of [Asp] along with the energy of the inter-conversion barrier

Intramolecular proton transfer		
Structure	ΔE (solvent $\epsilon = 35.7$) (kcal mol ⁻¹)	
	MP2/6-31+G**	PBE/6-311+G**
Asp-N	0.0	0.0
Asp-Z	1.2	-0.5
TS	0.8	0.1

expect to see a faster and more consistent isomerization. What we have instead seen is a much more interesting different situation where the proton is transferred between anions and intramolecular proton transfer within the same molecular ion is almost absent. There are two ways in which the proton can be transferred between the anions. The first one takes place between a carboxyl function and a carboxylate function, while the second sees the transfer from a carboxyl to an amino group. What we have seen in our simulations is the occurrence of the second mechanism.

We begin our analysis of the AIMD trajectory by looking at the RDFs of the possible H-bond contacts and of the center of mass (c.o.m.) of the molecular ions that are both reported in Fig. 6. If we look at the right panel we can see that in the case of [Ch][Asp] the average distance between the c.o.m.s of the anions (black line) is comparable to the average distance between the anions and the cations (blue line) or even lower. The average distance between cations is instead larger than the other two. In [Ch][Asp] we have again a situation where the “typical” IL structure characterized by a charge-alternating pattern of ions is heavily modified by the presence of strong H-bonds that connect the anionic moieties. These connections, which may



Scheme 3 Intramolecular proton transfer in the [Asp] anion.

promote intramolecular proton transfer, are exclusively located between anions whereby the cations seem to play a very limited role and act here almost as spectators. While we cannot be sure that all cations would behave in the same manner we are fairly sure that structurally similar cations (*e.g.* bulky molecular ions with a delocalized positive charge) should not partake in the proton transfer reaction directly.

In the left panel of Fig. 6, we have plotted the relevant RDFs for the geometric characterization of the complex H-bonding patterns. Most of the H-bonding features (blue line) connect the anions to the cations with an average C(O)O⁻⋯(H)-O distance of 2.7 Å. Two other kinds of H-bonds are present: the first one (black line) is formed between two anions and connects the carboxylate oxygen atoms to themselves; the second (red line) connects the carboxylate oxygen atoms to the nitrogen of the amino-group. Among the possible O-N contacts we have shown in the inset the two contributions due to the protonated and deprotonated carboxylate. As we see, the protonated carboxylate is the dominant configuration that is the one corresponding to the C(O)O-H⋯N arrangement. This is an important point because it shows how in these systems the amino-group acts almost exclusively as an acceptor of H-bonds and only marginally acts as a donor towards the negatively charged carboxylate.

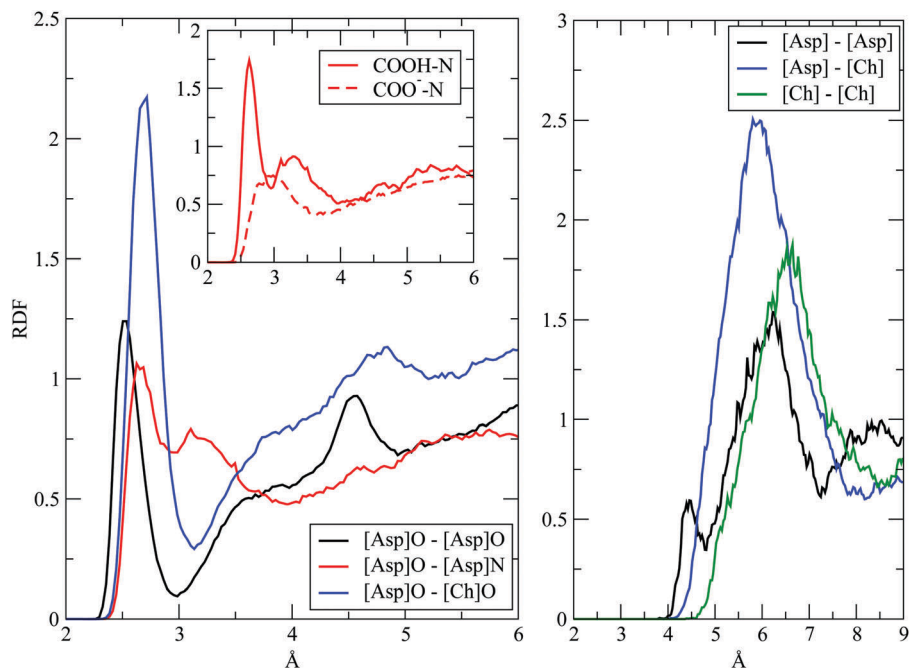


Fig. 6 [Ch][Asp]: left: intramolecular RDFs for the 3 possible H-bond contacts: black, between the carboxylates; red, between the carboxylates and the amino-group; blue, between the carboxylate and the hydroxyl. The inset shows the two possible [Asp][Asp] ON contacts, O–H–N with a proton (solid) and O–N without a proton (dashed). Right: Intramolecular RDFs for the centers of mass: between the anions (black), the cations (green) and cations and anions (blue).

Before proceeding to a discussion of the dynamics of protons in the simulation, we highlight the fact that during the time span of the simulation we do not see any intramolecular proton transfer. All the proton transfers that we have found

take place between different anions and we discover that in 4 anion–anion pairs (over a total of 16, *i.e.* the 25% of the anions) a proton is transferred from the carboxylate to the amino-group. In this respect, this liquid turns out to be radically

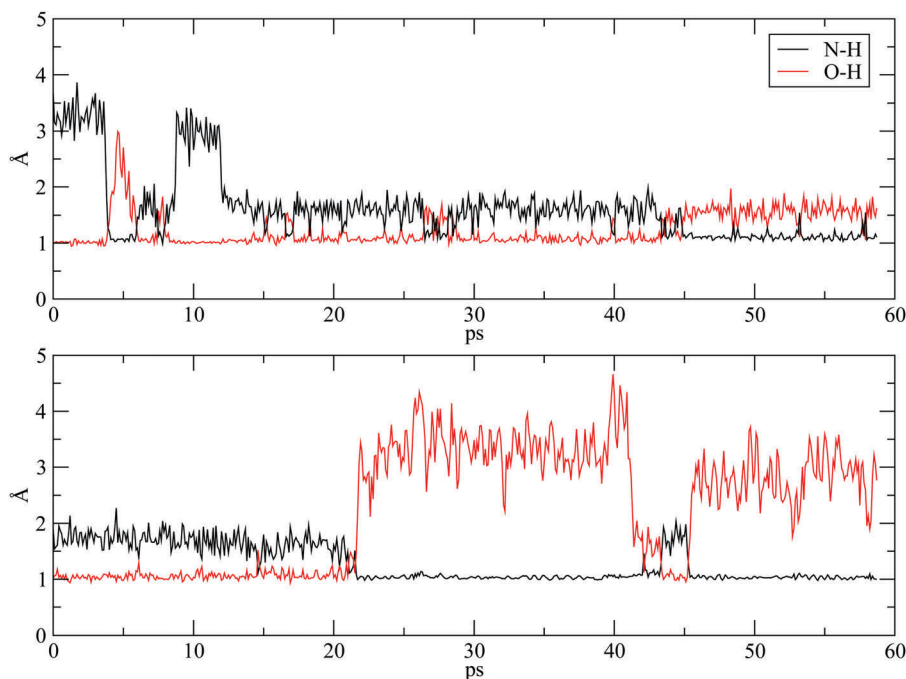


Fig. 7 [Ch][Asp]: intermolecular anion–anion N–H and O–H distances as a function of simulation time. The two panels depict two different proton transfer reactions.

different from the [Cys] based one and also a more promising candidate for proton conduction.

As an example, we have plotted the O–H and N–H distances for two inter-anionic proton transfer occurrences in Fig. 7. As we see in both cases we have an initial situation where the

proton is on the COO^- group and ends on the NH_2 group. The situation depicted by the upper panel is particularly interesting because, as shown by the corresponding snapshot sequence in Fig. 8, we have an initial situation (frame 1) where the anion interacts with the deprotonated COO^- group of another [Asp] anion.

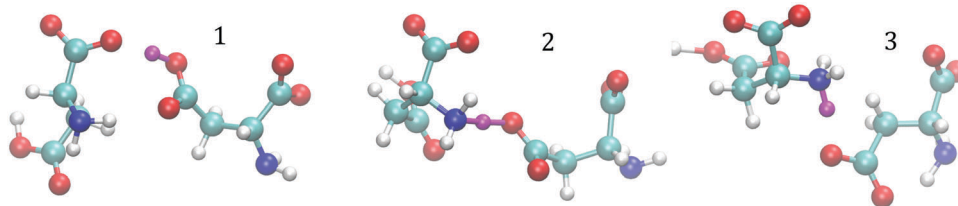


Fig. 8 [Ch][Asp]: sequential snapshots of a proton transfer from the COOH to the amino group.

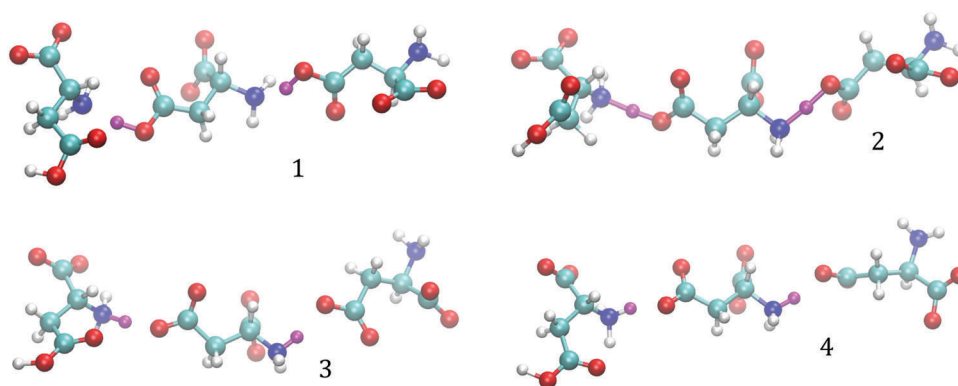


Fig. 9 [Ch][Asp]: sequential snapshots of a concerted proton transfer from two $-\text{COOH}$ groups towards two amino groups.

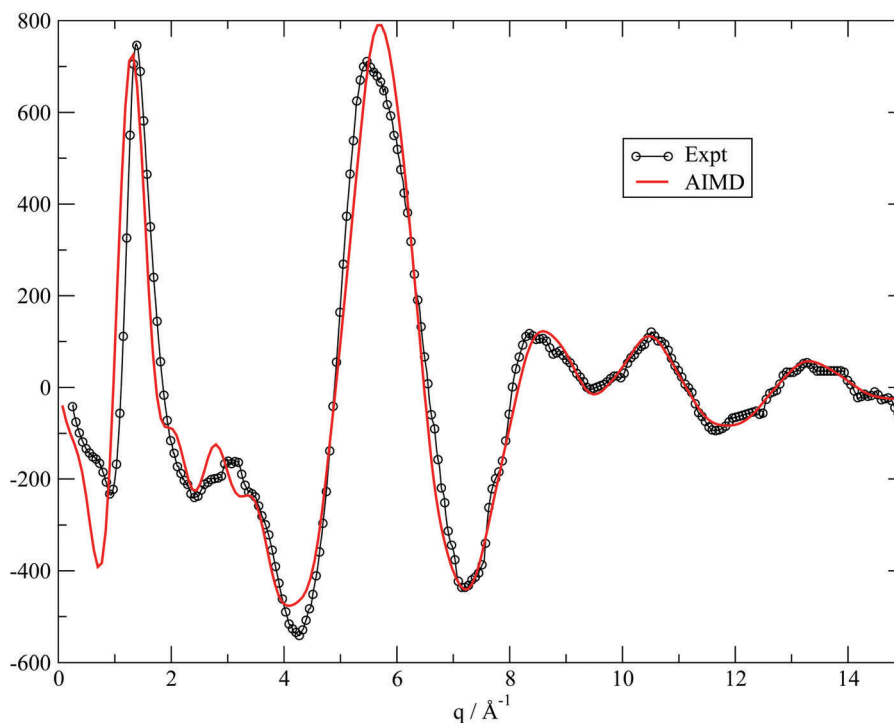


Fig. 10 [Ch][Asp]: $I(Q)M(Q)Q$ of the [Ch][Asp] system. Theoretical data are unreliable under 0.4 \AA^{-1} because of the finite size of the simulation cell.

Proton transfer does not occur between the carboxylates (as expected from pK_a values), but the anion undergoes rotation/displacement and the proton is finally transferred to the amino-group.

One of the most interesting cases of proton transfer is represented by the configurations sequentially depicted in Fig. 9 where we show the situation of three anions connected through H-bonds and where there is the simultaneous transfer of two protons between them. Initially (frame 1) the two protons are on the carboxyl groups. In frame 2 they are transferred simultaneously to the NH_2 . In frames 3 and 4 we see the reaction has completed.

The structure of the [Ch][Asp] IL is particularly intriguing as it results from our simulations because it seems to contain chains of anions interconnected by H-bonds along which proton transfer might occur quickly through jumps that are analogous to the “Grotthus” mechanism in water. The cation acts as a mere spectator.

3.4 [Ch][Asp] experimental validation

The experimental and computed $I(Q)M(Q)Q$ of the [Ch][Asp] system are reported in Fig. 10. From the data presented we clearly see that our simulation is able to grasp with very good accuracy the position of the heavy atoms (oxygen, carbon and nitrogen). Since in the hydrogen bonding network the heavy atoms distances are strongly dependent on the proton positions we conclude that the simulation data presented above represent a very reliable description of the true fluid at least from the point of view of its average geometrical structure. The small mismatch in the first peak at low Q is due to the intrinsic difficulty in determining the density of the experimental sample.

4. Conclusions and perspectives

The [Ch][Cys] and [Ch][Asp] PILs have been analyzed by means of state-of-the-art computational techniques. We have clearly identified in those materials several occurrences of proton transfer reactions that occur within or between anions. In particular, we have discovered that molecular ions composing the [Ch][Cys] liquid can undergo an isomerization reaction mediated by an intramolecular proton transfer from the $-SH$ to the amino-group. We have also shown that this isomerization reaction leads to a complex material where part of the anions is in an anion–zwitterionic form. This feature might be the microscopic driving force for the peculiar bulk state of analogous liquids where the amino-acid has a heteroatom in the side chain which turned out to have higher viscosities and densities with respect to the other amino-acids.

The [Ch][Asp] liquid, on the other hand, has clearly shown many occurrences of intermolecular proton transfer that takes place through the strong H-bonds existing between the protonated carboxylic group and the amino one. These H-bonds not only can promote charge transport, but bringing into close contact the anionic moieties, they can alter significantly the

common microscopic structure of ILs where normally anions and cations form a well-defined charge-alternating pattern.

While generally, PILs are ionic liquids formed through a quantitative acid–base reaction, where the transferred proton permanently resides on the cationic moiety (the base), the system examined here have both shown the possibility of triggering additional proton exchange reactions by means of the protons attached to the amino-acid side chains. It is well known that PILs are good candidates as solvents for electrochemical devices. The possibility, for these materials, of representing a viable route to an ideal situation where protons can find ways of moving through the fluid independently of the much slower molecular ions is therefore extremely appealing for electrochemical application. As stated by Belieres and Angell “a dry proton conductivity mechanism is one of “holy grails” of electrolyte science.”²⁰ From our results we conclude that, although to a limited extent, proton transfer mechanisms in neat, dry ionic liquids are possible and may open new routes for electrochemical applications where the need for high conductivity and stable non-aqueous media is a key objective.

Acknowledgements

The authors gratefully acknowledge Prof. Ruggero Caminiti (Sapienza University of Rome, Chemistry Department) for providing us with the experimental X-Ray diffraction patterns. EB, LG and MM acknowledge the financial support of the Scientific Committee of the University of Rome through grants C26A13KR5Z and C26A142SCB. EB acknowledges the computational support from Cineca (grant no. IsC20_AARTIL and IsCrC_POLIL) and PRACE (grant no. 2013091962).

References

- 1 D. H. Zaitsau, G. J. Kabo, A. A. Strechan, Y. U. Paulechka, A. Tschersich, S. P. Verevkin and A. Heintz, Experimental Vapor Pressures of 1-Alkyl-3-methylimidazolium Bis(trifluoromethylsulfonyl)imides and a Correlation Scheme for Estimation of Vaporization Enthalpies of Ionic Liquids, *J. Phys. Chem. A*, 2006, **110**, 7303–7306.
- 2 J. S. Wilkes, A short history of ionic liquids from molten salts to neoteric solvents, *Green Chem.*, 2002, **4**, 73–80.
- 3 T. Welton, Room-Temperature Ionic Liquid. Solvents for Synthesis and Catalysis, *Chem. Rev.*, 1999, **99**, 2071–2084.
- 4 P. Wasserscheid and W. Keim, Ionic liquids – new “solutions” for transition metal catalysis, *Angew. Chem.*, 2000, **39**, 3772–3789.
- 5 E. W. Castner and J. F. Wishart, Spotlight on ionic liquids, *J. Chem. Phys.*, 2010, **132**, 120901.
- 6 J. Stoimenovski, P. M. Dean, E. I. Izgorodina and D. R. MacFarlane, Protic Pharmaceutical Ionic Liquids and Solids: Aspects of Protonics, *Faraday Discuss.*, 2012, **154**, 335–352.
- 7 Y. Yu, X. Lu, Q. Zhou, K. Dong, H. Yao and S. Zhang, Biodegradable Naphthenic Acid Ionic Liquids: Synthesis,

- Characterization, and Quantitative Structure–Biodegradation Relationship, *Chem. – Eur. J.*, 2008, **14**, 11174–11182.
- 8 W. L. Hough, M. Smiglak, H. Rodríguez, R. P. Swatloski, S. K. Spear, D. Y. Daly, J. Pernak, J. E. Grisel, R. D. Carliss, M. D. Soutullo, J. H. Davis, Jr. and R. D. Rogers, The Third Evolution of Ionic Liquids: Active Pharmaceutical Ingredients, *New J. Chem.*, 2007, **31**, 1429–1436.
 - 9 Y. Fukaya, Y. Iizuka, K. Sekikawa and H. Ohno, Bio ionic liquids: room temperature ionic liquids composed wholly of biomaterials, *Green Chem.*, 2007, **9**, 1155–1157.
 - 10 K. Fukumoto, M. Yoshizawa and H. Ohno, Room Temperature Ionic Liquids from 20 Natural Amino Acids, *J. Am. Chem. Soc.*, 2005, **127**, 2398–2399.
 - 11 G. Masci, S. De Santis, F. Casciotta, R. Caminiti, E. Scarpellini, M. Campetella and L. Gontrani, Cholinium-Amino Acid based Ionic Liquids: a new method of synthesis and physico-chemical characterization, *Phys. Chem. Chem. Phys.*, 2015, **17**, 20687–20698.
 - 12 X. D. Hou, Q. P. Liu, T. J. Smith, N. Li and M. H. Zong, Evaluation of Toxicity and Biodegradability of Cholinium Amino Acids Ionic Liquids, *PLoS One*, 2013, **8**, 59145.
 - 13 K. D. Weaver, H. J. Kim, J. Sun, D. R. MacFarlane and G. D. Elliott, Cyto-toxicity and biocompatibility of a family of choline phosphate ionic liquids designed for pharmaceutical applications, *Green Chem.*, 2010, **12**, 507–513.
 - 14 P. Nockemann, B. Thijs, K. Driesen, C. R. Janssen, K. Van Hecke, L. Van Meervelt, S. Kossmann, B. Kirchner and K. Binnemans, Choline Saccharinate and Choline Acesulfamate: Ionic Liquids with Low Toxicities, *J. Phys. Chem. B*, 2007, **111**, 5254–5263.
 - 15 J.-C. Plaquevent, J. Levillain, F. Guillen, C. Malhiac and A. C. Gaumont, Ionic Liquids: New Targets and Media for Amino Acid and Peptide Chemistry, *Chem. Rev.*, 2008, **108**, 5035–5060.
 - 16 M. Petkovic, J. L. Ferguson, H. Q. N. Gunaratne, R. Ferreira, M. C. Leitao, K. R. Seddon, L. P. N. Rebelo and C. S. Pereira, Novel biocompatible cholinium-based ionic liquids-toxicity and biodegradability, *Green Chem.*, 2010, **12**, 643–649.
 - 17 G.-h. Tao, L. He, W.-s. Liu, L. Xu, W. Xiong, T. Wang and Y. Kou, Preparation, characterization and application of amino acid-based green ionic liquids, *Green Chem.*, 2006, **8**, 639–646.
 - 18 T. L. Greaves and C. J. Drummond, Protic Ionic Liquids: Evolving Structure–Property Relationships and Expanding Applications, *Chem. Rev.*, 2015, **115**, 11379–11448.
 - 19 E. Bodo, A. Sferrazza, R. Caminiti, S. Mangialardo and P. Postorino, A prototypical ionic liquid explored by *ab initio* molecular dynamics and Raman spectroscopy, *J. Chem. Phys.*, 2013, **139**, 144309.
 - 20 J.-F. Belieres and C. A. Angell, Protic Ionic Liquids: Preparation, Characterization, and Proton Free Energy Level Representation, *J. Phys. Chem. B*, 2007, **111**, 4926–4937.
 - 21 T. L. Greaves, K. Ha, B. W. Muir, S. C. Howard, A. Weerawardena, N. Kirby and C. J. Drummond, Protic ionic liquids (PILs) nanostructure and physicochemical properties: development of high-throughput methodology for PIL creation and property screens, *Phys. Chem. Chem. Phys.*, 2015, **17**, 2357.
 - 22 E. Bodo, S. Mangialardo, F. Capitani, L. Gontrani, F. Leonelli and P. Postorino, Interaction of a Long Alkyl Chain Protic Ionic Liquid and Water, *J. Chem. Phys.*, 2014, **140**, 204503.
 - 23 M. Campetella, L. Gontrani, F. Leonelli, L. Bencivenni and R. Caminiti, Two Different Models to Predict Ionic-Liquid Diffraction Patterns: Fixed-Charge *versus* Polarizable Potentials, *ChemPhysChem*, 2015, **16**, 197–203.
 - 24 K. Fumino, V. Fossog, P. Stange, D. Paschek, R. Hempelmann and R. Ludwig, Controlling the Subtle Energy Balance in Protic Ionic Liquids: Dispersion Forces Compete with Hydrogen Bonds, *Angew. Chem., Int. Ed.*, 2015, **54**, 2792–2795.
 - 25 H. Doi, X. Song, B. Minofar, R. Kanzaki, T. Takamuku and Y. Umebayashi, A New Proton Conductive Liquid with No Ions: Pseudo-Protic Ionic Liquids, *Chem. – Eur. J.*, 2013, **19**, 11522–11526.
 - 26 J. Stoimenovski, E. I. Izgorodina and D. R. MacFarlane, Ionicity and proton transfer in protic ionic liquids, *Phys. Chem. Chem. Phys.*, 2010, **12**, 10341–10347.
 - 27 J. Stoimenovski, E. I. Izgorodina and D. R. MacFarlane, Ionicity and proton transfer in protic ionic liquids, *Phys. Chem. Chem. Phys.*, 2010, **12**, 10341–10347.
 - 28 W. Xu and C. A. Angell, Solvent-Free Electrolytes with Aqueous Solution-Like Conductivities, *Science*, 2003, **302**, 422–425.
 - 29 D. A. Case, T. A. Darden, T. E. Cheatham, C. L. Simmerling, J. Wang, R. E. Duke, R. Luo, R. C. Walker, W. Zhang, K. M. Merz, B. Roberts, S. Hayik, A. Roitberg, G. Seabra, J. Swails, A. W. Goetz, I. Kolossváry, K. F. Wong, F. Paesani, J. Vanicek, R. M. Wolf, J. Liu, X. Wu, S. R. Brozell, T. Steinbrecher, H. Gohlke, Q. Cai, X. Ye, J. Wang, M. J. Hsieh, G. Cui, D. R. Roe, D. H. Mathews, M. G. Seetin, R. Salomon-Ferrer, C. Sagui, V. Babin, T. Luchko, S. Gusarov, A. Kovalenko and P. A. Kollman, *Amber 12*, 2012.
 - 30 J. Wang, R. M. Wolf, J. W. Caldwell, P. A. Kollman and D. A. Case, Development and testing of a general amber force field, *J. Comput. Chem.*, 2004, **25**, 1157–1174.
 - 31 J. Wang, W. Wang, P. A. Kollman and D. A. Case, Automatic atom type and bond type perception in molecular mechanical calculations, *J. Mol. Graphics Modell.*, 2006, **25**, 247–260.
 - 32 M. Campetella, E. Bodo, M. Montagna, S. De Santis and L. Gontrani, Theoretical study of ionic liquids based on the cholinium cation. *Ab initio* simulations of their condensed phases, *J. Chem. Phys.*, 2016, **144**, 104504.
 - 33 J. Hutter, M. Iannuzzi, F. Schiffmann and J. VandeVondele, cp2k: atomistic simulations of condensed matter systems, *Wiley Interdiscip. Rev.: Comput. Mol. Sci.*, 2013, **4**, 15–25.
 - 34 J. Vandevondele, M. Krack, F. Mohamed, M. Parrinello, T. Chassaing and J. Hutter, Fast and accurate density functional calculations using a mixed Gaussian and plane waves approach, *Comput. Phys. Commun.*, 2005, **167**, 103–128.
 - 35 J. VandeVondele and J. Hutter, An efficient orbital transformation method for electronic structure calculations, *J. Chem. Phys.*, 2003, **118**, 4365–4369.

- 36 G. K. H. Madsen, Functional form of the generalized gradient approximation for exchange: The PBE functional, *Phys. Rev. B: Condens. Matter Mater. Phys.*, 2007, **75**, 195108.
- 37 S. Grimme, Semiempirical GGA-Type Density Functional Constructed with a Long-Range Dispersion Correction, *J. Comput. Chem.*, 2006, **27**, 1787–1789.
- 38 S. Goedecker, M. Teter and J. Hutter, Separable dual-space Gaussian pseudopotentials, *Phys. Rev. B: Condens. Matter Mater. Phys.*, 1996, **54**, 1703–1710.
- 39 C. Hartwigsen, S. Goedecker and J. Hutter, Relativistic separable dual-space Gaussian pseudopotentials from H to Rn, *Phys. Rev. B: Condens. Matter Mater. Phys.*, 1998, **58**, 3641–3662.
- 40 W. G. Hoover, Canonical dynamics: Equilibrium phase-space distributions, *Phys. Rev. A: At., Mol., Opt. Phys.*, 1985, **31**, 1695–1697.
- 41 J. Hutter, A. Alavi, T. Deutsch, M. Bernasconi, S. Goedecker, D. Marx, M. Tucker-man and M. Parrinello, *CPMD version 3.9.1*, IBM Research Division, IBM Corp and Max Planck Institute Stuttgart, 2004.
- 42 M. Campetella, L. Gontrani, E. Bodo, A. Martino, F. D'Apuzzo, S. Lupi and R. Caminiti, Interaction and dynamics of ionic liquids based on Choline and amino-acids anions, *J. Chem. Phys.*, 2015, **142**, 234502.
- 43 N. Trouillier and J. L. Martins, Efficient Pseudopotentials for Plane-Wave Calculations, *Phys. Rev. B: Condens. Matter Mater. Phys.*, 1991, **43**, 1993.
- 44 R. Caminiti, private communication.
- 45 M. Brehm and B. Kirchner, TRAVIS – A Free Analyzer and Visualizer for Monte Carlo and Molecular Dynamics Trajectories, *J. Chem. Inf. Model.*, 2011, **51**, 2007–2023.
- 46 M. J. Frisch, G. W. Trucks, H. B. Schlegel, G. E. Scuseria, M. A. Robb, J. R. Cheeseman, G. Scalmani, V. Barone, B. Mennucci, G. A. Petersson, H. Nakatsuji, M. Caricato, X. Li, H. P. Hratchian, A. F. Izmaylov, J. Bloino, G. Zheng, J. L. Sonnenberg, M. Hada, M. Ehara, K. Toyota, R. Fukuda, J. Hasegawa, M. Ishida, T. Nakajima, Y. Honda, O. Kitao, H. Nakai, T. Vreven, J. A. Montgomery, Jr., J. E. Peralta, F. Ogliaro, M. Bearpark, J. J. Heyd, E. Brothers, K. N. Kudin, V. N. Staroverov, R. Kobayashi, J. Normand, K. Raghavachari, A. Rendell, J. C. Burant, S. S. Iyengar, J. Tomasi, M. Cossi, N. Rega, J. M. Millam, M. Klene, J. E. Knox, J. B. Cross, V. Bakken, C. Adamo, J. Jaramillo, R. Gomperts, R. E. Stratmann, O. Yazyev, A. J. Austin, R. Cammi, C. Pomelli, J. W. Ochterski, R. L. Martin, K. Morokuma, V. G. Zakrzewski, G. A. Voth, P. Salvador, J. J. Dannenberg, S. Dapprich, A. D. Daniels, Ö. Farkas, J. B. Foresman, J. V. Ortiz, J. Cioslowski and D. J. Fox, *Gaussian 09, Revision E.01*, Gaussian, Inc., Wallingford, CT, 2009.
- 47 V. R. Albertini, L. Bencivenni, R. Caminiti, F. Cilloco and C. Sadun, A new technique for the study of phase transitions by means of energy dispersive X-ray diffraction. Application to polymeric samples, *J. Macromol. Sci., Part B: Phys.*, 1996, **35**, 199–213.
- 48 M. Carbone, R. Caminiti and C. Sadun, Structural study by energy dispersive X-ray diffraction of amorphous mixed hydroxycarbonates containing Co, Cu, Zn, Al, *J. Mater. Chem.*, 1996, **6**, 1709–1716.
- 49 D. Atzei, T. Ferri, C. Sadun, P. Sangiorgio and R. Caminiti, Structural characterization of complexes between iminodiacetate blocked on styrene-divinylbenzene matrix (Chelex 100 resin) and Fe(III), Cr(III), and Zn(II) in solid phase by energy-dispersive X-ray diffraction, *J. Am. Chem. Soc.*, 2001, **123**, 2552–2558.
- 50 L. Gontrani, O. Russina, F. C. Marincola and R. Caminiti, An energy dispersive x-ray scattering and molecular dynamics study of liquid dimethyl carbonate, *J. Chem. Phys.*, 2009, **131**, 244503.
- 51 A. Benedetto, E. Bodo, L. Gontrani, P. Ballone and R. Caminiti, Amino Acid Anions in Organic Ionic Compounds. An ab Initio Study of Selected Ion Pairs, *J. Phys. Chem. B*, 2014, **118**, 2471–2486.
- 52 M.-M. Huang, Y. Jiang, P. Sasisanker, G. W. Driver and H. Weingärtner, Static Relative Dielectric Permittivities of Ionic Liquids at 25 °C, *J. Chem. Eng. Data*, 2011, **56**, 1494–1499.
- 53 J. Zheng, Y. Zhao and D. G. Truhlar, Representative Benchmark Suites for Barrier Heights of Diverse Reaction Types and Assessment of Electronic Structure Methods for Thermochemical Kinetics, *J. Chem. Theory Comput.*, 2007, **3**, 569–582.